Atmospheric Research 301 (2024) 107268

Contents lists available at ScienceDirect

Atmospheric Research

journal homepage: www.elsevier.com/locate/atmosres

Performance of DSCOVR/EPIC diurnal aerosol products over China: Ground validation and intercomparison

Lu Gui [a], Minghui Tao [a], Lina Xu [b,*], Yi Wang [a], Jun Wang [c], Lunche Wang [a], Liangfu Chen [d]

[a] Hubei Key Laboratory of Regional Ecology and Environmental Change, School of Geography and Information Engineering, China University of Geosciences, Wuhan 430074, China
[b] Subsurface Multi-scale Imaging Key Laboratory, School of Geophysics and Geomatics, China University of Geosciences, Wuhan 430074, China
[c] Center for Global and Regional Environmental Research, The University of Iowa, Iowa City, IA 52242, USA
[d] State Key Laboratory of Remote Sensing Science, Aerospace Information Research Institute, Chinese Academy of Sciences, Beijing 100101, China

ARTICLE INFO

Keywords:
Diurnal aerosol products
EPIC
Validation
China

ABSTRACT

The Earth Polychromatic Imaging Camera (EPIC) provides an unprecedented diurnal global observation of aerosol variations since 2015. In this study, we present a comprehensive insight into the performance and application of EPIC aerosol products over China from near-UV (EPICAERUV) and Multi-Angle Implementation of Atmospheric Correction (EPIC MAIAC) algorithms. Despite a consistency with AERONET observation, EPICAERUV AOD exhibits systematic overestimation in low-moderate values (<0.5) in northern China with larger bias in the northwestern deserts. By contrast, EPIC MAIAC AOD exhibits a reliable performance in the whole China region but gets poorer than EPICAERUV retrievals in Xuzhou, Taihu and Hongkong due to different aerosol models used. Both EPICAERUV and EPIC MAIAC AOD can generally reproduced diurnal aerosol variations in ground observations. Furthermore, near-hour EPIC Ultraviolet Aerosol Index (UVAI) can clearly give the development and transport process of dust plumes and fire smoke over China. EPICAERUV Single Scattering Albedo (SSA) has 58.4% (43.0%) retrievals within expected error envelop of ±0.03 against AERONET Level 2.0 and 1.5 inversions respectively. The comparison of EPICAERUV and EPIC MAIAC algorithm shows that EPIC aerosol retrievals can be improved by utilizing combined UV and visible measurements with sensitivity to aerosol absorption and surface reflectance respectively. The unique advantages of EPIC's diurnal observations as well sensitivity to aerosol absorption and height exhibit great potential in updating global aerosol information.

1. Introduction

Atmospheric aerosols play a crucial role in the climate system by altering radiation budget of the Earth-atmosphere and modifying cloud properties (Kaufman et al., 2002). Moreover, numerous epidemiological studies have shown robust correlations between exposure levels of particle pollution and the morbidity and mortality of chronic respiratory diseases (Pope et al., 2002). Owing to short lifetimes and diverse sources, the concentration and composition of aerosols have a very inhomogeneous distribution over space and time, which exert a great challenge on quantifying their global climate and environmental effects (Mishchenko et al., 2004). Therefore, accurate observation of aerosol properties with sufficient spatial and temporal resolution is a fundamental requirement in climate and air quality studies.

Due to the growing recognition of the importance of global aerosol properties for climate change studies, dedicated satellite instruments with polar orbit are springing up since late 1990s. Satellite observations such as Moderate Resolution Imaging Spectrometer (MODIS), Multi-angle Imaging Spectrometer (MISR), and Polarization and Directionality of the Earth's Reflectances (POLDER) have greatly updated knowledge concerning global aerosol distribution and emission hotspots (Mishchenko et al., 2007). Considering the large diurnal variability of aerosols due to dynamic planetary boundary layer, outside transport, and chemical reactions (Gui et al., 2022; Lu et al., 2023; Wang et al., 2020, 2021), satellite observations with high temporal resolution is needed. Geostationary satellites such as Himawari-8, Geostationary Environment Monitoring Spectrometer (GEMS), and Tropospheric Emissions: Monitoring of Pollution (TEMPO) can provide hourly observations of aerosols (Bessho et al., 2016; Kim et al., 2020; Zhang et al., 2019). However, geostationary satellite observations are fixed in certain

* Corresponding author at: NO. 388, Lumo Road, Hongshan District, Wuhan 430074, China.
E-mail address: xulina@cug.edu.cn (L. Xu).

https://doi.org/10.1016/j.atmosres.2024.107268
Received 28 June 2023; Received in revised form 9 January 2024; Accepted 19 January 2024
Available online 28 January 2024

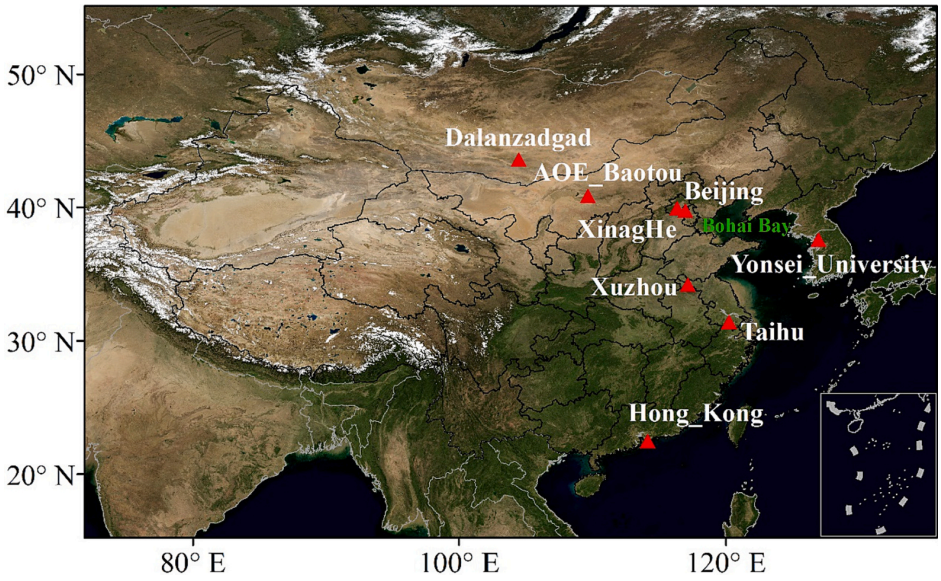

Fig. 1. Geographic location of AERONET sites (red) in MODIS RGB image derived from spectral surface reflectance after atmospheric correction. (For interpretation of the references to color in this figure legend, the reader is referred to the web version of this article.)

regions such as China or North America with a lack of global coverage.

To obtain a time-resolved global detection of daytime aerosols, cloud, and trace gases, Earth Polychromatic Imaging Camera (EPIC) onboard the Deep Space Climate Observatory (DSCOVR) spacecraft was launched in February 2015. The EPIC instrument takes a set of ten spectral images of entire sunlit face of Earth every 68 min in the Northern Hemisphere (NH) summer and 110 min in the winter, from Earth-Sun Lagrange-1 (L-1) point 1.5 $\times$ 10^6 km away (Herman et al., 2018). EPIC provides an unprecedented opportunity to explore diurnal variations of global aerosol properties (Marshak et al., 2018; Lu et al., 2023). In particular, EPIC measurements at ultraviolet (UV) and oxygen A and B bands are sensitive to absorbing aerosols such as airborne dust and fire smoke as well as their layer height (Ahn et al., 2021; Xu et al., 2017, 2019). However, performance and application potential of EPIC aerosol retrievals have been rarely examined in regional scales.

In this study, we present a comprehensive analysis of the performance and diurnal variations of EPIC aerosol retrievals over China by ground-based validations with the Aerosol Robotic Network (AERONET) inversions and inter-comparison with polar-orbiting satellite products. Section 2 introduces satellite products and AERONET inversions used in our study. The performance of EPIC Aerosol Optical Depth (AOD) is shown in Section 3.1. Then, EPIC Single Scattering Albedo (SSA) and Aerosol Layer Height (ALH) is evaluated in Section 3.2. Diurnal variations of typical dust and smoke transport events are analyzed in Section 3.3. Section 4 summarizes our findings and primary conclusions.

2. Data and methods

2.1. EPIC measurement

In June 2015, the DSCOVR satellite reached its destination at the L1 point, where EPIC provides spectral measurement of the entire sunlit face of Earth. EPIC measures top-of-atmosphere reflectance in 10 narrow bands centered at 317.3, 325, 340, 388, 443, 551, 680, 687.75, 764, and 779.5 nm. The EPIC observations can be used to retrieve ozone, aerosols, cloud, vegetation properties (Herman et al., 2018). EPIC spectral measurements have a spatial resolution of 18 km at nadir except 8 km at 443 nm (Ahn et al., 2021).

2.2. EPICAERUV algorithm

By utilizing spectral measurements at 340 and 388 nm that not sensitive to non-snow/ice surfaces, the EPIC near-UV aerosol algorithm (EPICAERUV) retrieves AOD/SSA at 388 nm and reports both retrievals at 340 nm and 500 nm based on the spectral model assumed in the inversion (Ahn et al., 2021). Meanwhile, a qualitative parameter, UV Aerosol Index (UVAI) is derived from contrast of EPIC observation at 340 nm and the Mie cloud calculations mixed with the pure Rayleigh atmosphere (Torres et al., 2018). UVAI is available over all conditions including snow/ice surface and clouds and even for aerosols mixed with clouds, which has been widely used to identify the presence of UV-absorbing aerosols (Torres et al., 2007).

For retrieval of EPICAERUV AOD and SSA, aerosols are assumed to be one of the three types including spherical carbonaceous, urban-industrial aerosols, and non-spherical desert dust with a fixed bi-modal size distribution and the real component of refractive index derived from climatology of AERONET inversions (Ahn et al., 2021). Then, aerosol type is determined by the combination of UVAI and AIRS carbon monoxide (CO) (Torres et al., 2013). Surface albedo and ALH is assumed as known by utilizing multi-year dataset of minimum reflectivity observations from OMI (Ozone Monitoring Instrument) and combinations of monthly CALIOP (Cloud-Aerosol Lidar with Orthogonal Polarization) ALH and transport model simulations respectively. The surface albedo database used in the EPICAERUV algorithm is based on a combination of TOMS (Total Ozone Mapping Spectrometer) (340 nm) and OMI (388 nm) sensors with a coarse spatial resolution at 0.5° $\times$ 0.5°. Since scattering parameters of each aerosol type at various scenarios have been pre-calculated in look-up tables (LUTs), AOD and SSA can be retrieved by matching spectral EPIC reflectance at top of atmosphere (TOA) with calculated ones. To consider the influence of subpixel cloud contamination, EPIC aerosol products utilize quality assurance (QA) flag to indicate the confidence level of retrieved parameters. A QA flag of 0 (FinalAlgorithmFlags = 0) denotes retrievals minimally affected by subpixel cloud contamination that is suitable for scientific use. Here we used the quality flag 0 to select the best retrievals in EPIC Level (L) 2 files.

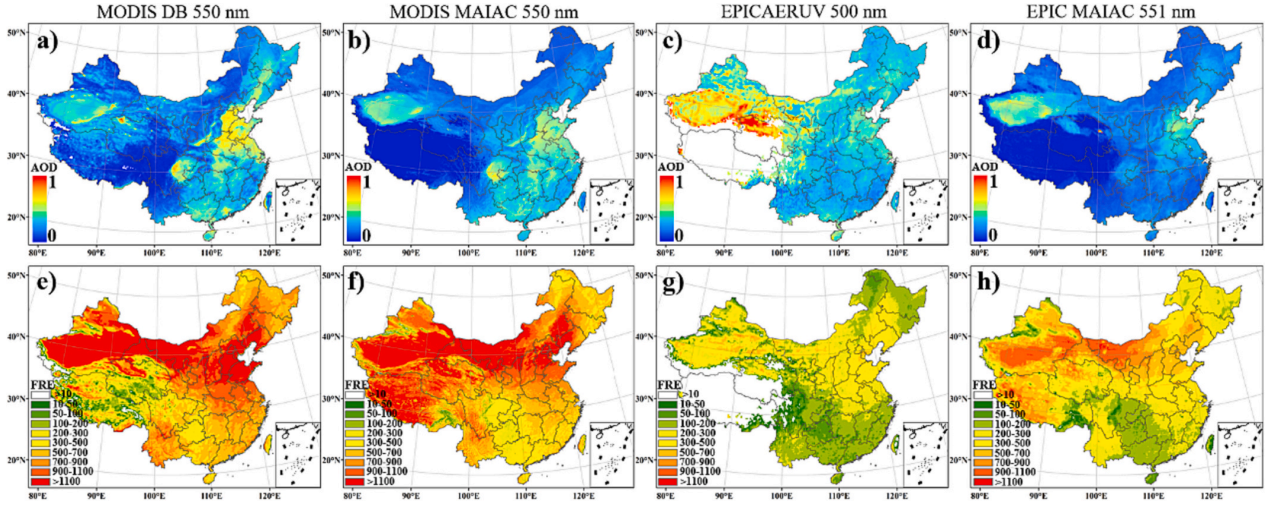

Fig. 2. Annual mean (top) and retrieval frequency (bottom) respectively for a) MODIS DB AOD, b) MODIS MAIAC AOD, c) EPICAERUV AOD, and d) EPIC MAIAC AOD at noon during 2016–2018 and 2020–2022.

2.3. EPIC MAIAC algorithm

In addition, NASA's Multi-Angle Implementation of Atmospheric Correction (MAIAC) algorithm is also applicable to DSCOVR/EPIC data (Lyapustin et al., 2021). Retrieval of Spectral Regression Coefficient (SRC) is an extremely important component of MAIAC, separating the surface and atmospheric signals from Top of Atmosphere Reflectance (TOA) measurements. Since EPIC lacks the 2130 nm band used by MAIAC MODIS, the SRC is defined as the ratio of surface reflectance in Blue to Red bands ($SRC = \rho_{L,Blu}/\rho_{L,Red}$). The MAIAC utilizes minimal ratio of spectral reflectance (443/680 nm) in 2-month period of time to estimate the SRC, and the AOD is obtained by matching the observed values with the theoretical TOA reflectance at 443 nm based on the look-up table. The eight prescribed regional aerosol models are used to represent the variability of aerosol properties over the global land. At high altitudes (>3.5 km, e.g., the Tibetan Plateau), the accuracy of the MAIAC AOD retrieval is insufficient, assuming a fixed AOD = 0.02 for the atmospheric correction (Lyapustin et al., 2021).

2.4. AERONET aerosol products

AERONET is a global ground-based remote sensing network of sun photometers providing highly accurate measurements and retrievals of aerosol optical and microphysical properties (Giles et al., 2019). By measuring direct sunlight under cloud-free conditions, AERONET can obtain spectral AOD with a very low uncertainty (~0.01 for visible and near infrared and ~ 0.02 for UV channels) (Eck et al., 1999), which is commonly taken as "ground truth" in evaluation of satellite retrievals. In combination with directional skylight measurements, aerosol micro-physical parameters including complex refractive index, volume size distribution, and non-spherical fraction are inversed (Dubovik et al., 2000), from which SSA and scattering phase function can be calculated.

We select the recent Version (V) 3 AERONET products for validation (Giles et al., 2019). The V3 Level (L) 1.5 AERONET products include automatic cloud screening and quality control, with additional pre-field and post-field calibration for L2.0 products. Owing to limited information content, AERONET SSA is selected for $AOD_{440} > 0.4$ and solar zenith angle (SZA) >50° (or > 25° for hybrid measurements) in L2.0 inversions, with estimated uncertainty within ±0.03 (Dubovik et al., 2002). By contrast, L1.5 AERONET SSA is not screened by AOD and SZA with larger uncertainties. Although there are many AERONET sites in China, only a few have continuous and long-term observations (Fig. 1). The V3 Level 2.0 AERONET product is preferable, and L1.5 data are used when the Level 2.0 results are not available. Similar as previous studies (Ahn et al., 2021), mean values of EPIC AOD from a spatial window of 5 × 5 pixels with AERONET site centered in are compared with AERONET measurements in a 10-min window of satellite overpass time. For validation of EPIC SSA, a 30-min time window of the satellite passing time is used. To compare with AERONET SSA at 440 nm, EPIC SSA is converted to 440 nm with linear interpolation of its retrievals at 388 and 500 nm.

2.5. CALIOP aerosol profile

The CALIOP aboard Cloud-Aerosol Lidar and Infrared Pathfinder Satellite Observation (CALIPSO), launched in April 2006 and concluded its science mission on August 1, 2023, provides vertical detection of backscattered signals of aerosol and clouds at 532 nm and 1064 nm, with polarization measurement at 532 nm (Liu et al., 2008). The standard EPICAERUV aerosol product employed in the current analysis does provide the effective ALH from the 30-month-long CALIOP-OMI dataset (Torres et al., 2013). For the validation of EPIC ALH, we select Version 4.10 CALIOP Level 2 aerosol extinction profiles at 532 nm. To match with EPIC ALH, we used the mean extinction height calculated from the CALIOP extinction profiles (Koffi et al., 2012):

$$ALH_{CALIOP} = \frac{\sum_{i=1}^{n} \beta_{ext,i} Z_i}{\sum_{i=1}^{n} \beta_{ext,i}} \quad (1)$$

Here, $\beta_{ext,i}$ is the aerosol extinction coefficient at 532 nm at level i, and Z_i is the altitude (km) of level i. Thus, ALH_{CALIOP} represents an effective ALH weighted by the aerosol extinction at each level and is consistent with ALH defined in the EPIC algorithm (Torres et al., 2013).

2.6. MODIS aerosol products

By utilizing pre-calculated database of spectral surface reflectance, MODIS Deep Blue (DB) algorithm has a reliable AOD retrieval in global scale (Hsu et al., 2013). Ground-based validations show that MODIS DB AOD has a robust performance in high-AOD conditions over East Asia (Tao et al., 2019). Moreover, MODIS Multi-angle Implement of Atmospheric Correction (MAIAC) algorithm provides accurate AOD retrieval at 1 km by utilizing minimum reflectance ratio (Lyapustin et al., 2018). MAIAC and ground-observed AOD values show high correlation coefficient of ~0.94 in two AERONET sites of Beijing and XiangHe (Tao et al., 2019). Here we select the 10 km Collection (C) 6.1 MODIS DB and 1 km

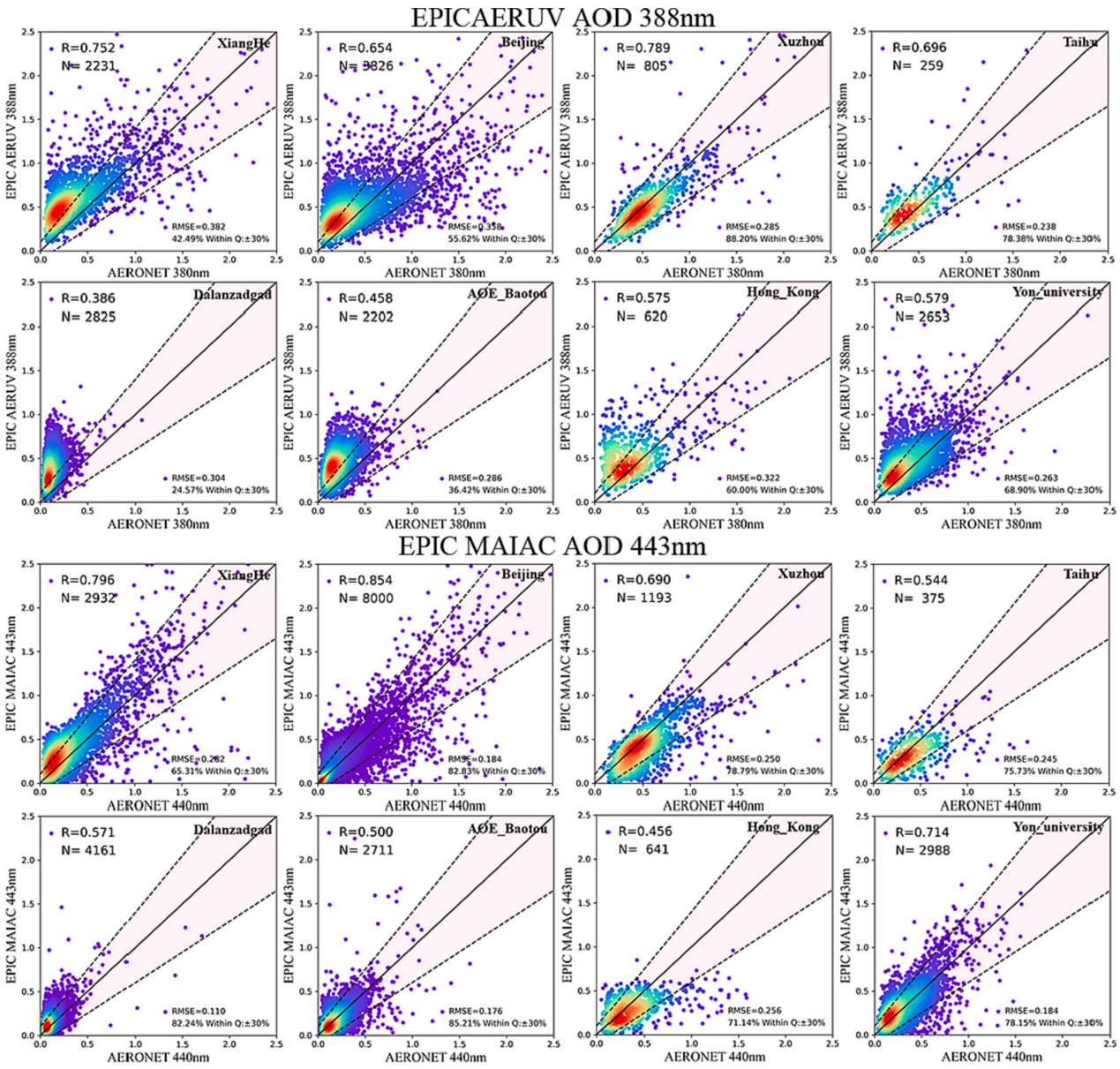

Fig. 3. Scatter plots of hourly EPIC and AERONET AOD during 2015–2022.

C6 MAIAC AOD at 550 nm with best retrieval quality to make an inter-comparison with EPIC results.

2.7. OMPS aerosol products

In October 2011, the hyperspectral instrument of Ozone Mapping and Profiler Suite (OMPS) on board the Suomi National Polar-orbiting Partnership (NPP) satellite was launched. The OMPS hyperspectral instrument measured the complete spectrum within 300–380 nm at an average spectral resolution of 1.1 nm and a spatial resolution of 50 km at nadir. Based on the differences of molecular scattering and in aerosol absorption in the UV band, the OMPS UVAI is a widely used indicator for the existence of UV-absorbing aerosols, such as elevated dust and biomass burning smoke (Torres et al., 2007). Despite a qualitative parameter, UVAI is very sensitive to elevated dust and smoke, becomes higher for absorbing aerosols above or even mixed with clouds due to enhanced absorption (Tao et al., 2021, 2022).

3. Results and analysis

3.1. General performance of different EPIC AOD products over China

To assess the performance of EPIC AOD in China, Fig. 2 shows the annual mean of EPIC and MODIS AOD along with their corresponding retrieval frequency. Both EPIC and MODIS algorithms retrieve AOD over cloud-free and snow/ice-free surfaces, but their retrievals exhibit distinct spatial patterns. Compared with MODIS DB and MAIAC AOD at 550 nm, EPICAERUV AOD at 500 nm and EPIC MAIAC AOD at 551 nm obviously underestimate aerosol loading in eastern China and overestimate AOD values in the northwest, especially in the Taklamakan Desert. Owing to a much lower spatial resolution than MODIS's, EPIC pixels are easier to be contaminated by clouds. Though EPIC AOD near

Table 1
Statistical measures of EPIC-AERONET AOD comparison for selected AERONET sites.

Site name	EPICAERUV				EPIC MAIAC			
	N	R	RMSE	Q	N	R	RMSE	Q
XinagHe	2231	0.752	0.382	42.49%	2932	0.796	0.282	65.31%
Beijing	3826	0.654	0.358	55.62%	8000	0.854	0.184	82.83%
Xuzhou	805	0.789	0.285	88.20%	1193	0.690	0.250	78.79%
Taihu	259	0.696	0.238	78.38%	375	0.544	0.245	75.73%
Dalanzadgad	2825	0.386	0.304	24.57%	4161	0.571	0.110	82.24%
AOE_Baotou	2202	0.458	0.286	36.42%	2711	0.500	0.176	85.21%
Hong_Kong	620	0.575	0.322	60.00%	641	0.456	0.256	71.14%
Yon_university	2652	0.579	0.263	68.90%	2988	0.714	0.184	78.15%

Notes. Acronyms: N-number of matchups, R-correlation, RMSE-root-mean-square-error, Q-% AOD matchups falling within 30% uncertainty.

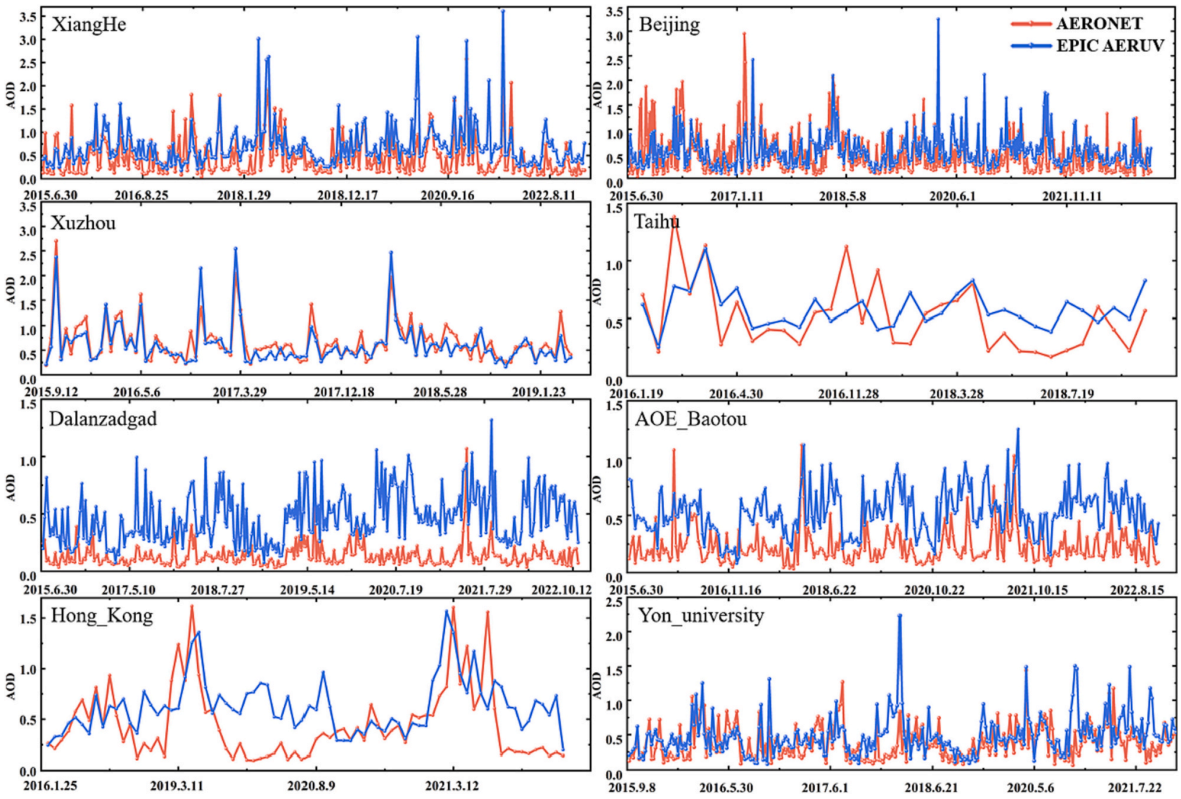

Fig. 4. Daily EPICAERUV AOD at 388 nm and AERONET AOD at 380 nm in eight AERONET sites.

noon has a lower retrieval frequency than matched MODIS products, the diurnal EPIC observations enable a much higher frequency of aerosol retrievals.

Fig. 3 shows validation of the different EPIC AOD products at six AERONET sites in China and two adjacent sites. The dotted line indicates 1:1 agreement level, and the solid lines denote the expected error of ±30% or 0.1 of AERONET AOD, whichever is larger. In Table 1, N represents the total number of hourly coincident AOD data, the correlation coefficient (R), Q is the percent of EPIC AOD data falling within the expected error envelope and the root mean square error (RMSE). Despite a consistency with AERONET observation, there is a large overestimation for low-moderate values (<0.5) of EPICAERUV AOD at 388 nm in northern China, which is much higher over bright surface in the northwest. EPICAERUV AOD retrievals become very scattered in high values (>0.5) and tend to have a systematic underestimation (Table.S1).

By contrast, EPIC MAIAC AOD at 443 nm exhibits a reliable performance in the whole China region, especially at Beijing, where R reaches 0.854. In Xuzhou, Taihu and Hong Kong, performance of MAIAC AOD gets poorer than EPICAERUV retrievals due to different aerosol modes used. At lower AODs, the error in surface albedo and its spectral dependence at two channels (340–388 nm) drives the retrieval bias of EPICAERUV AOD, whereas at higher aerosol loading, aerosol layer height and aerosol type both determine the accuracy of the EPICAERUV AOD retrievals. Meanwhile, the uncertainties of surface SRC and aerosol model are the main sources of errors of EPIC MAIAC AOD in China.

To further examine the performance of EPIC retrieval, Fig. 4 shows comparison of collocated daily AOD values from EPICAERUV (388 nm) and AERONET (380 nm) during 2015–2022. Despite considerable bias in ground validation, daily variations of EPICAERUV retrievals are very consistent with AERONET AOD in eastern China, which can well capture daily fluctuation of aerosol loading. However, EPICAERUV AOD are much higher than the low values of AERONET in arid regions and desert. By contrast, daily variation of EPIC MAIAC (443 nm) has higher

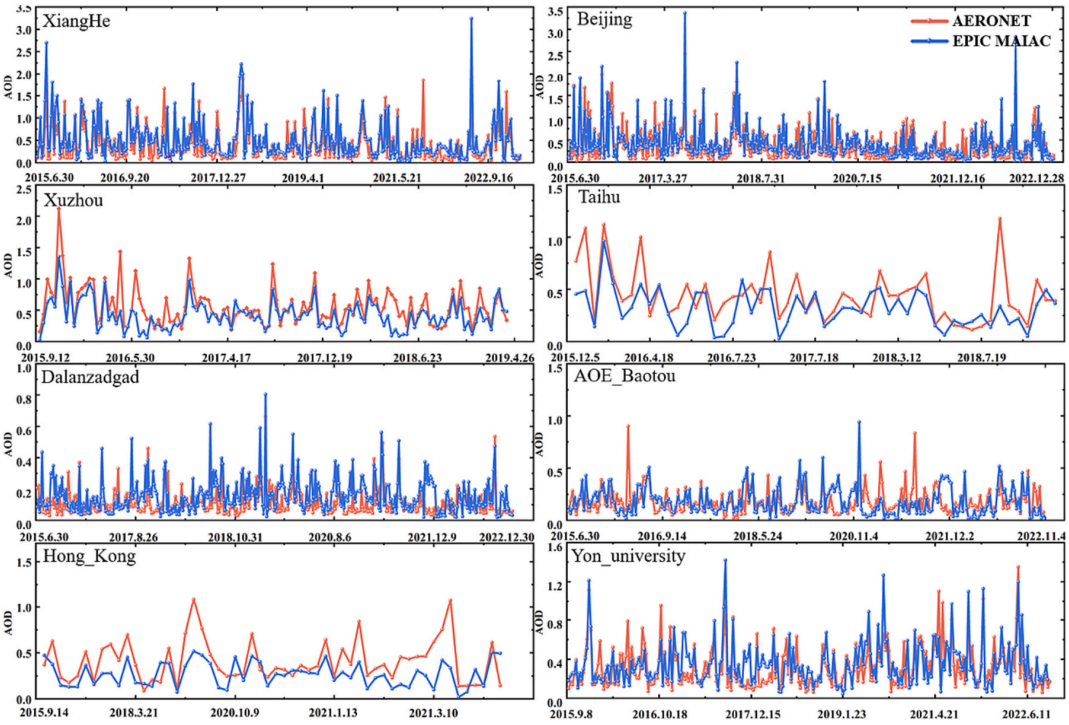

Fig. 5. Daily EPIC MAIAC AOD at 443 nm and AERONET AOD at 440 nm in eight AERONET sites.

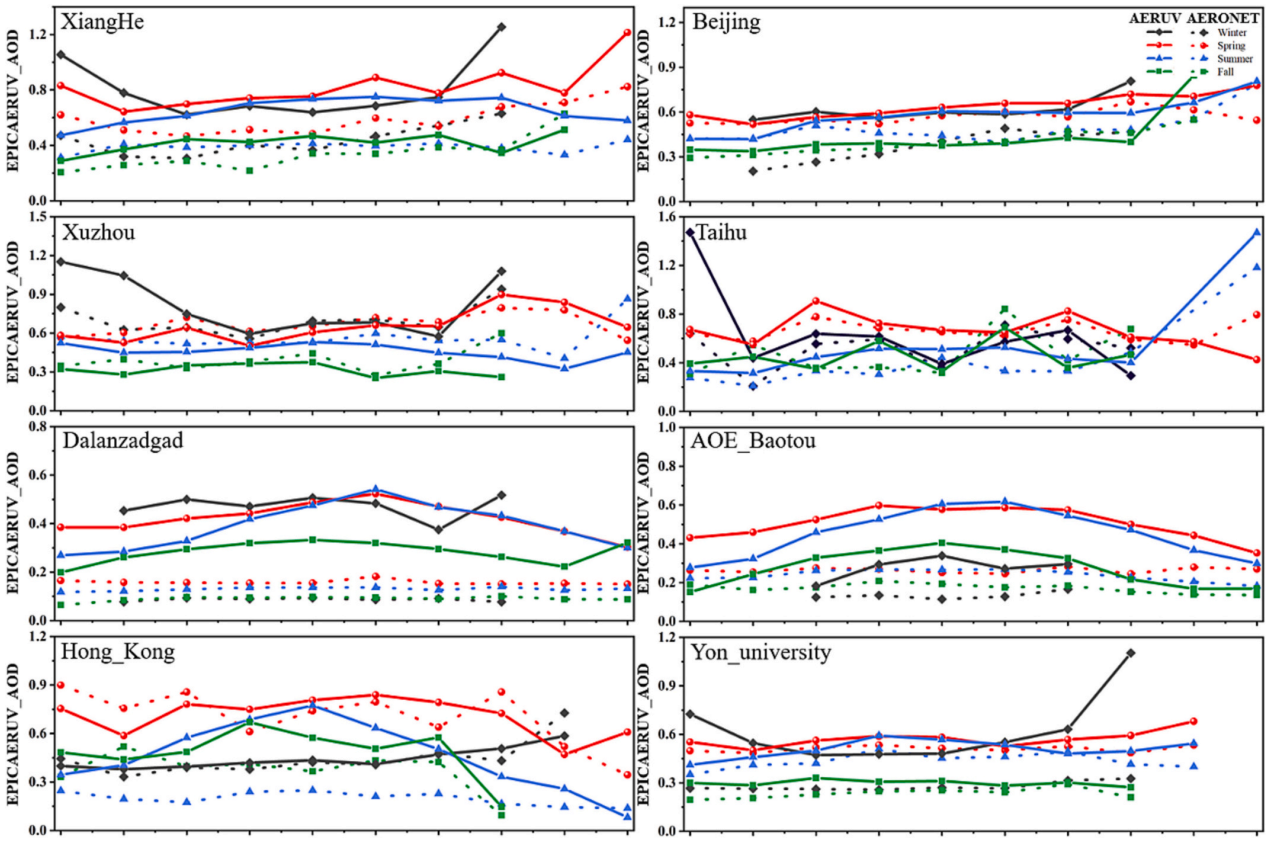

Fig. 6. Diurnal variations of hourly EPICAERUV (solid line) and AERONET (dotted line) AOD at eight sites in different seasons during 2015 to 2022.

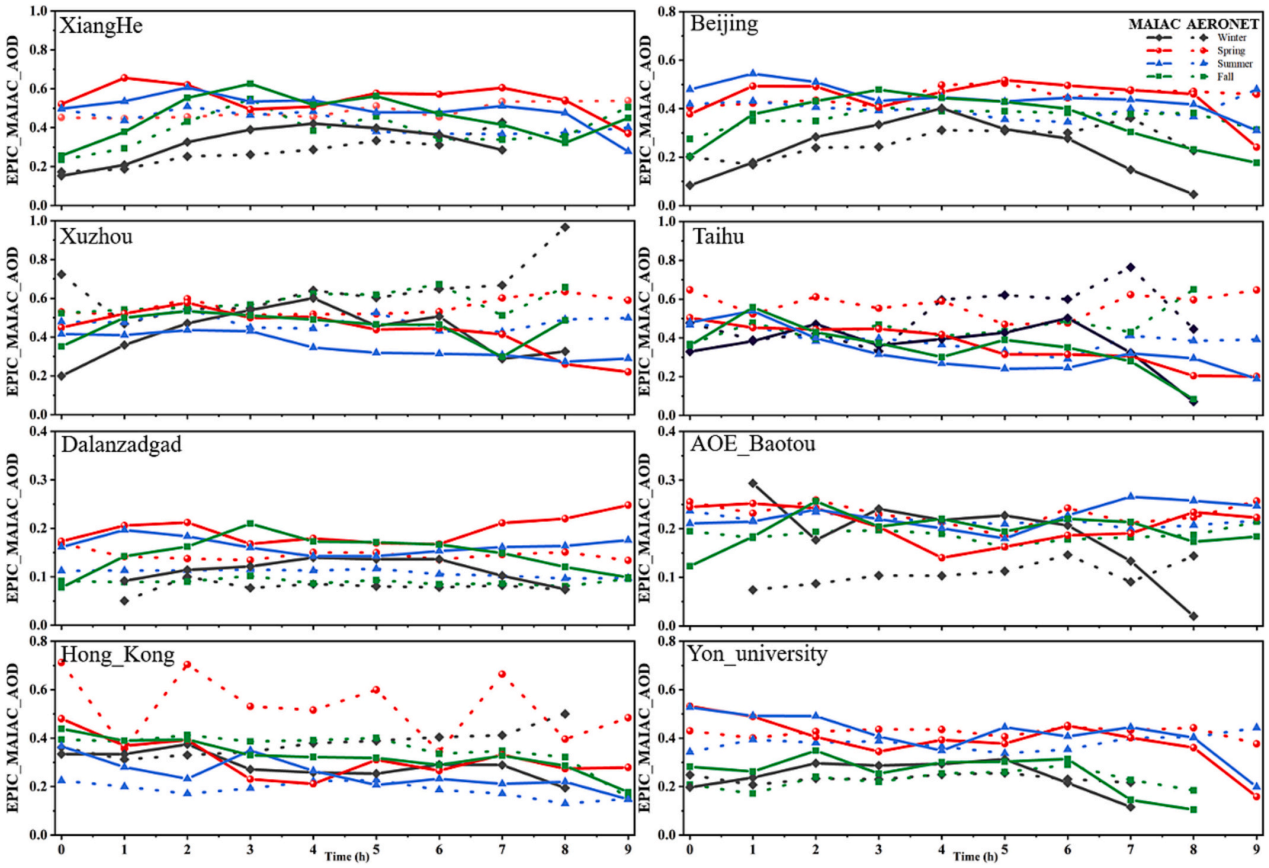

Fig. 7. Diurnal variations of hourly EPIC MAIAC (solid line) and AERONET (dotted line) AOD at eight sites in different seasons during 2015 to 2022.

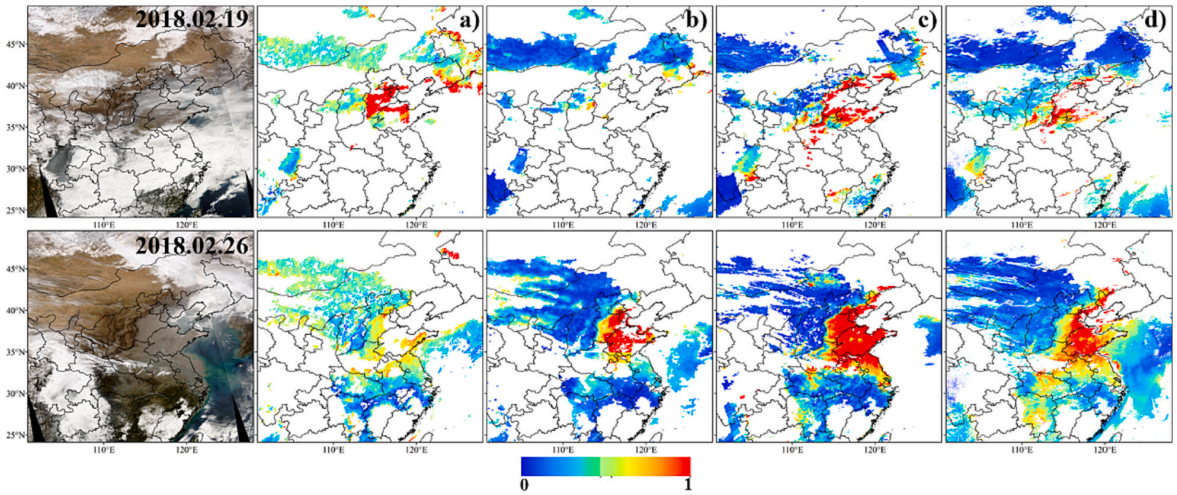

Fig. 8. (a) EPICAERUV AOD at 500 nm, (b) EPIC MAIAC AOD at 551 nm, (c) MODIS DB AOD at 550 nm, and (d) MODIS MAIAC AOD at 550 nm on 19 and 26 Feb 2018, respectively.

consistency than AERONET AOD (440 nm) during the same period (Fig. 5).

The unique advantage of the EPIC measurement is the diurnal observation of aerosol variations. Compared with AERONET AODs, the EPIC retrievals clearly show the diurnal variability of aerosol loading in the eastern part (Fig. 6). For instance, EPICAERUV AOD at 388 nm can well capture the peak values of aerosol loading at early morning and late afternoon in northern China during winter. AERONET AOD in the northwest exhibits no obvious diurnal variations and the influence of dust events can be smoothed out by the seasonal mean values. Owing to large bias over bright surfaces, diurnal EPICAERUV AOD is not consistent with AERONET values.

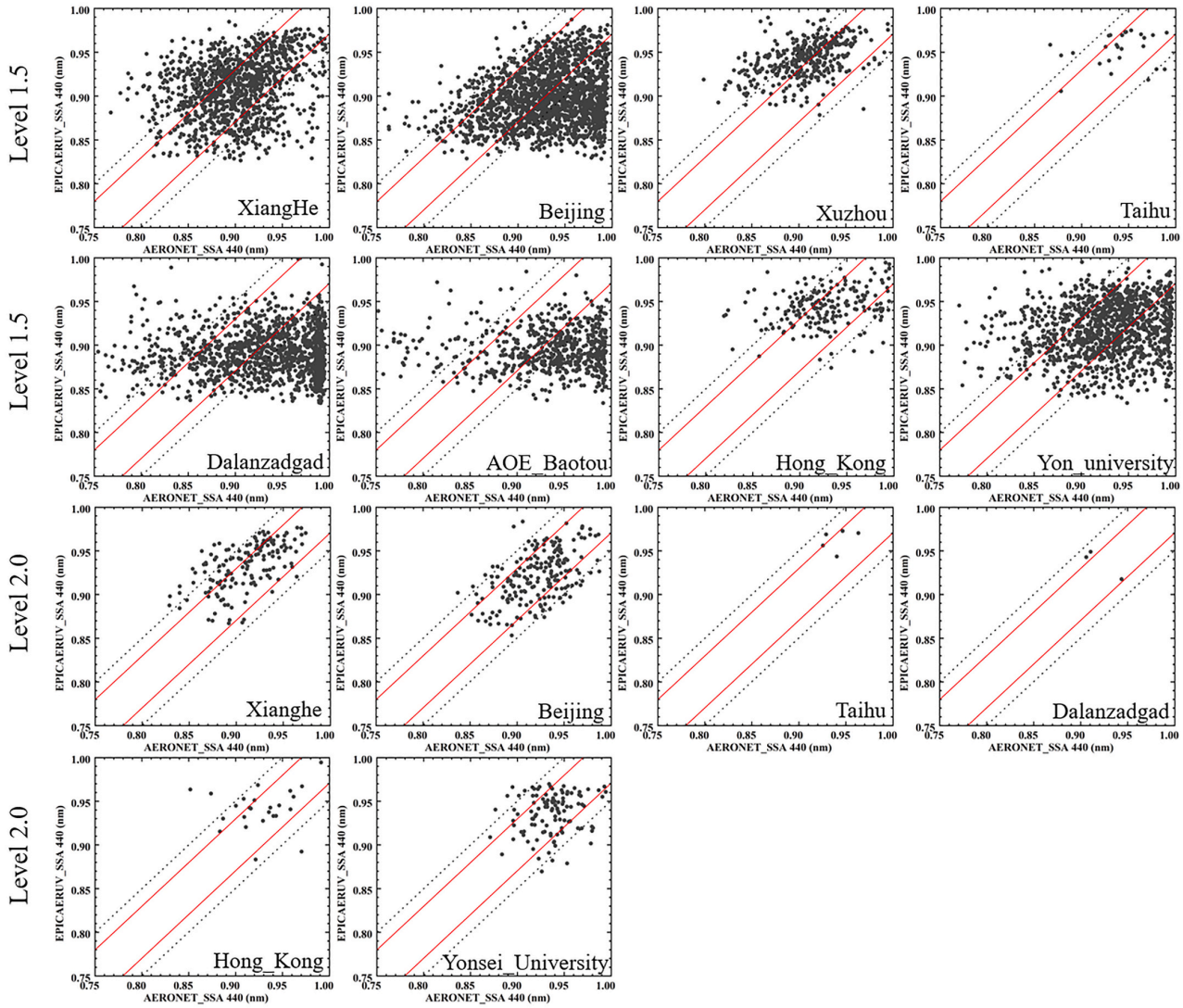

Fig. 9. Scatter plots of EPICAERUV with L2.0 and L1.5 AERONET SSA at 440 nm.

Table 2
Statistical measures of EPIC-AERONET SSA comparison for selected AERONET sites.

	Site name	N	R	RMSE	$SD_{(EPIC)}$	$M_{(EPIC)}$	$SD_{(AERONET)}$	$M_{(AERONET)}$	Q_0.03	Q_0.05
Level 1.5	XinagHe	1157	0.280	0.046	0.034	0.912	0.041	0.902	51.1%	73.6%
	Beijing	1856	0.242	0.057	0.031	0.896	0.044	0.936	38.6%	60.9%
	Xuzhou	387	0.446	0.047	0.021	0.943	0.034	0.907	42.6%	68.7%
	Taihu	26	0.218	0.036	0.019	0.956	0.030	0.943	65.4%	80.8%
	Dalanzadgad	1254	0.036	0.076	0.027	0.888	0.061	0.943	25.6%	41.7%
	AOE_Baotou	619	0.027	0.075	0.024	0.892	0.063	0.943	25.5%	44.8%
	Hong_Kong	197	0.236	0.047	0.022	0.944	0.043	0.926	50.8%	78.7%
	Yon_university	1221	0.166	0.052	0.031	0.920	0.046	0.932	44.6%	66.9%
Level 2.0	XinagHe	154	0.593	0.035	0.026	0.937	0.032	0.912	60.4%	86.4%
	Beijing	201	0.514	0.029	0.028	0.921	0.030	0.926	69.7%	91.5%
	Taihu	5	0.355	0.026	0.011	0.969	0.013	0.940	60.0%	100.0%
	Dalanzadgad	3	0.955	0.034	0.014	0.943	0.017	0.911	33.3%	100.0%
	Hong_Kong	25	0.141	0.040	0.023	0.943	0.032	0.924	60.0%	88.0%
	Yon_university	112	0.188	0.030	0.023	0.941	0.025	0.937	67.0%	88.4%

Notes. Acronyms: N-number of matchups, R-correlation, RMSE-root-mean-square-error, SD-standard deviation, M-median, Q_0.03 and Q_0.05-% SSA matchups falling within an absolute difference of 0.03 and 0.05.

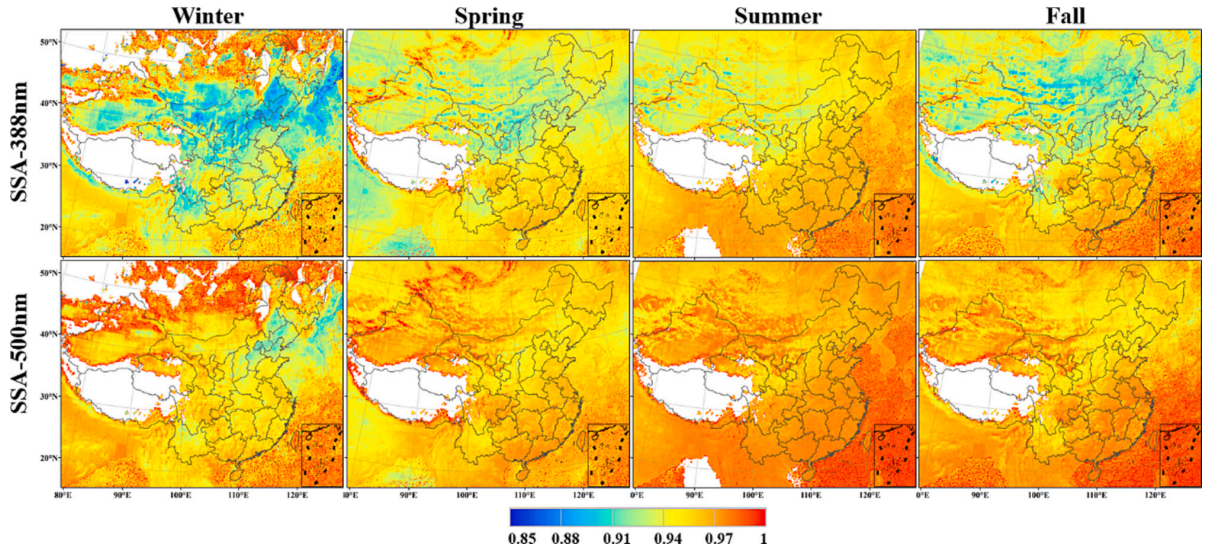

Fig. 10. Seasonal distribution of EPICAERUV 388 nm and 500 nm SSA in winter, spring, summer, and fall of 2015–2022.

The EPIC MAIAC AOD at 443 nm shows the peak values of aerosol loading around noon in North China during winter (Fig. 7). By contrast, the diurnal variation of MAIAC AOD is more consistent with AERONET AOD at eight sites. To further examine performance of EPIC retrievals in regional scales, daily map of EPIC and MODIS AOD is compared over eastern China (Fig. 8). While the spatial patterns of EPIC and MODIS AOD is at very close levels in eastern China, abnormal high values of EPICAERUV AOD are prevalent in the deserts and arid regions. The contamination of cloud and edges of snow/ice surface can be an important cause.

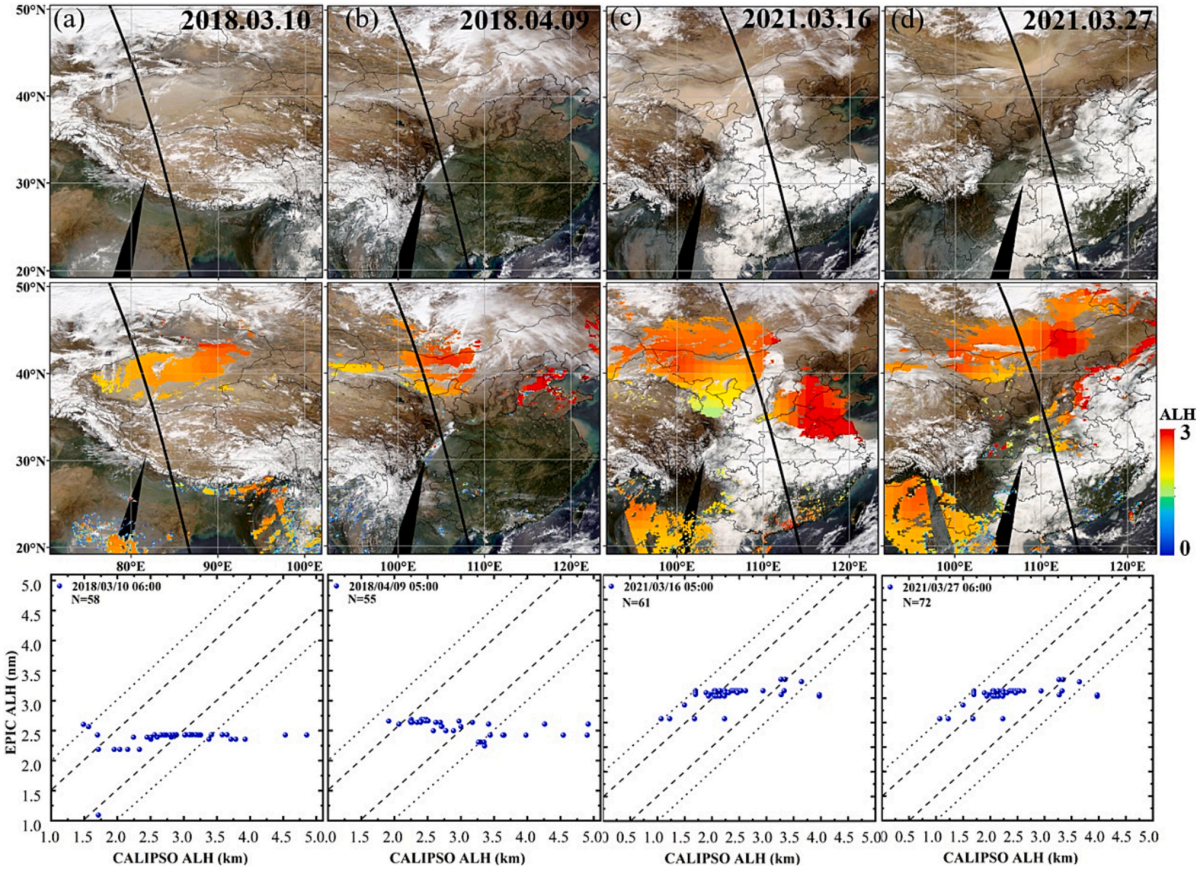

Fig. 11. Terra MODIS true color images (top), and EPIC ALH (middle), and comparison of EPIC and CALIOP ALH (bottom). The black line denotes CALIOP track.

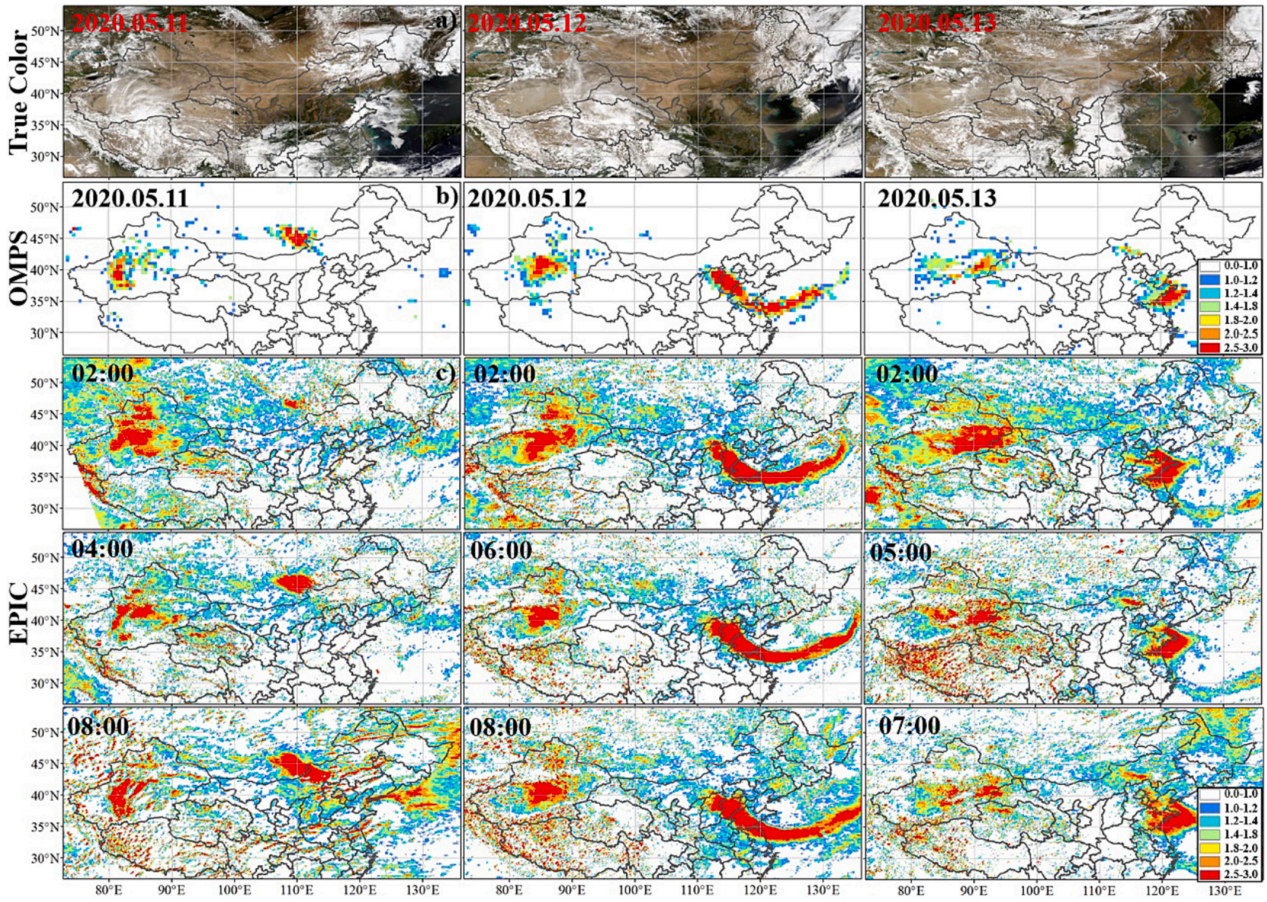

Fig. 12. Suomi NPP/VIIRS true color images, OMPS UV aerosol index (UVAI), and hourly EPIC UVAI during May 11–13, 2020.

3.2. Evaluation of EPICAERUV SSA and ALH

Fig. 9 displays comparison of EPIC SSA at 440 nm with L2.0 and 1.5 AERONET inversions respectively as well as corresponding statistics in Table 2. Compared with L2.0 AERONET inversion, EPIC SSA exhibits a reliable performance, with 60%–69.7% retrievals falling within expected error envelope of ±0.03 except 33.3% Dalanzadgad site. By the prior information including UVAI and AIRS CO, EPIC UV measurements can enable a quantitative retrieval of SSA. As a LUT-based aerosol algorithm, retrieval accuracy of EPIC SSA is largely influenced by assumed microphysical parameters of the aerosol types as well as prescribed surface albedo and ALH (Ahn et al., 2021). EPIC SSA retrievals in the northwest are relatively underestimated compared to those of AERONET, which is closely connected with the large overestimation of EPIC AOD. By contrast, EPIC SSA has a much poorer accuracy in validation with L1.5 AERONET inversion. There are only 38.6% EPIC SSA values falling within expected error envelope of ±0.03 in Beijing site. It should be stated that EPIC SSA has a better performance at Taihu site in comparison with L1.5 AERONET (65.4%) rather than 2.0 (60.0%). The considerable uncertainties in EPIC retrievals and AERONET inversions in low-AOD conditions can both contribute to the notable difference of EPIC SSA from L2.0 and 1.5 AERONET inversions.

Seasonal mean of EPIC SSA at 388 and 500 nm during 2015 to 2022 exhibits a well self-consistent spatial pattern over China (Fig. 10). Similar as previous studies (Tao et al., 2020), aerosol absorption gets weaker obviously from concentrated industrial regions in northern China to southern China, especially during the coal-burning for heating season in winter. By contrast, EPIC SSA is highest in summer, when hygroscopic growth of scattering particles in high relative humidity conditions. Abnormal values exist in EPIC SSA over the edges of deserts and snow/ice regions in the northwest, where EPIC retrievals have large bias.

To evaluate the influence of ALH on EPIC retrieval, EPIC ALH is compared with daily CALIPSO observation in several typical events (Fig. 11). Considering the large daily and diurnal variations of ALH (Gui et al., 2022), monthly climatology of CALIPSO ALH cannot well represent the actual situations. While daily CALIPSO ALH changes between 1.0 and 5.0 km, EPIC ALH is fixed around 2.5 or 3.0 km, which can be one of the important error sources of AOD and SSA retrievals, with an underestimation (overestimation) in ALH yields higher (lower) AODs and lower (higher) SSAs (Jethva et al., 2014). It's worth noting that most EPIC ALH values are around 3 km in low-AOD conditions, which has prevalent overestimation.

3.3. Application of EPICAERUV observations over China

Although EPIC aerosol retrievals are subject to considerable uncertainties, hourly EPIC UVAI can give diurnal variations of absorbing aerosols such as dust transport (Fig. 12). Compared with hyperspectral satellite instruments such as from OMPS and OMI, EPIC has a finer spatial resolution and larger wavelength width with higher signal-noise ratio. The hourly EPIC UVAI clearly shows the evolution process of one dust event from morning to the late afternoon in the Gobi deserts on May 11, 2020. With the high temporal resolution, EPIC UVAI not only gives spatial variations of the dust transport, but can also identify dust sources from diurnal changes of dust plumes. Compared with OMPS UVAI, EPIC

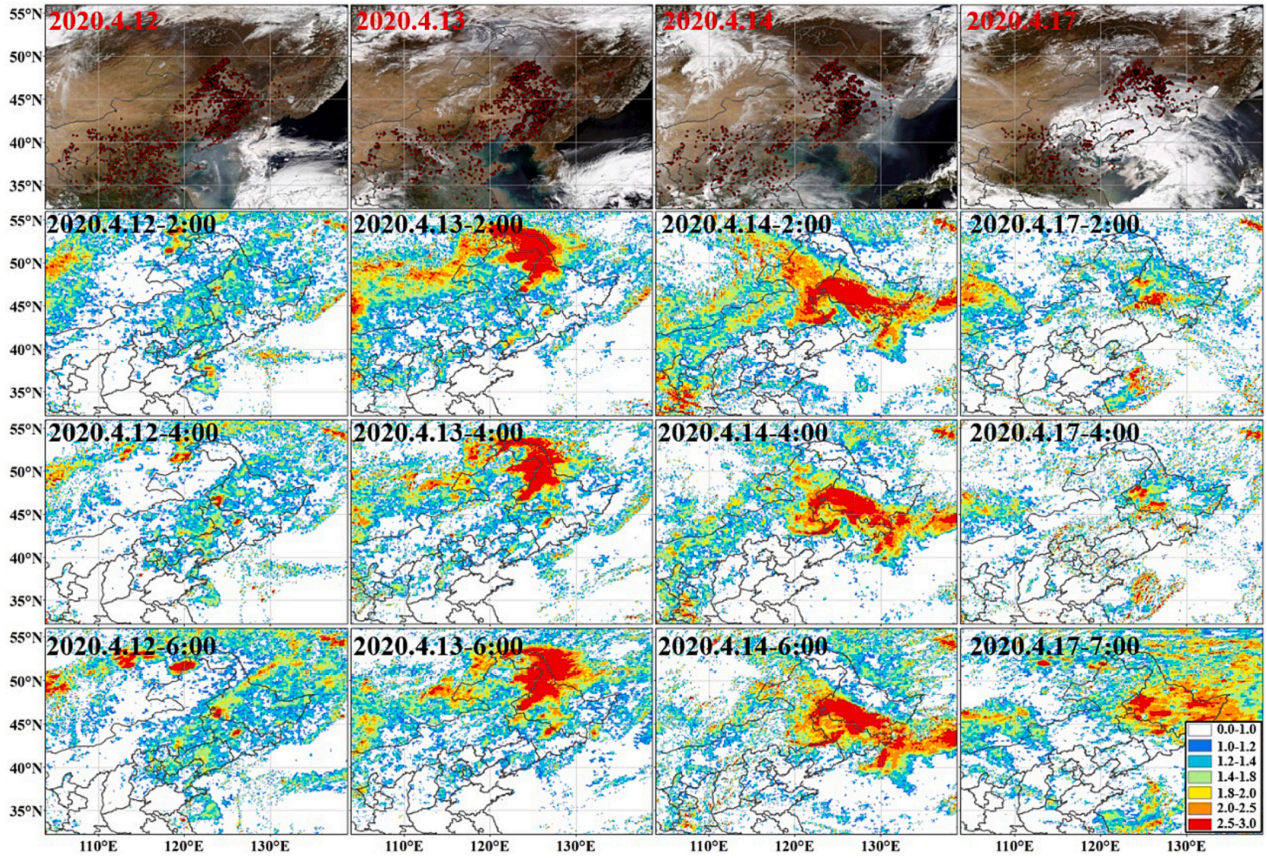

Fig. 13. Suomi NPP/VIIRS true color images with fires (red dots), and hourly EPIC UVAI during April 12–14 and 17, 2020. (For interpretation of the references to color in this figure legend, the reader is referred to the web version of this article.)

observation is more sensitive to the existence of airborne dust at low concentrations.

The diurnal variations of EPIC UVAI are sensitive to local biomass burning emissions. During the agricultural burning season in the northwest, EPIC UVAI can well reflect spatial variations of the fire smoke (Fig. 13). The prevailing agricultural fires are concentrated in the northwest on April 12, 2020, and their emissions have been transported southerly to the Bohai Bay. Fire emissions are blown to northern part in the night, and dense smoke appears on the next day. Compared with notable diurnal variations of absorbing aerosol over the Gobi deserts, spatial movement of the smoke plumes are much slower during April 13–14, which is mainly driven by daily changes of large-scale airflows. When strong winds come on April 17, fire smoke can be blown downstream within several hours.

4. Conclusions

The DSCOVR/EPIC provides a unique diurnal-resolved global aerosol observation. In this study, we present a comprehensive insight into performance of two EPIC aerosol algorithms and their application over China. EPICAERUV AOD agrees well with AERONET observations in Xuzhou, Taihu, and Hongkong, but has considerable overestimation over Beijing and XiangHe as well as bright surface in the northwestern deserts and arid regions. By contrast, EPIC MAIAC AOD utilizing visible bands exhibits a generally good performance in the whole China, especially at the Beijing, where R reaches 0.854. In Xuzhou, Taihu and Hong Kong, the performance of MAIAC AOD gets poorer than EPICAERUV retrievals due to different aerosol modes used. Moreover, EPICAERUV SSA exhibits a very consistent variation with AERONET inversions. Hourly EPICAERUV UVAI can clearly capture spatial variations and evolution process of dust events and fire smoke over China.

The diurnal EPIC measurements have large potential in quantifying global aerosol loading of typical types and their spatial variations. However, EPICAERUV retrievals utilize only two UV bands with prescribed aerosol models, surface albedo, and ALH, which have obvious uncertainties over China. Meanwhile, the uncertainties of surface SRC and aerosol model are the main sources of errors of EPIC MAIAC AOD in China. While EPIC visible and NIR measurements include more information from surface contribution, the UV bands are sensitive to aerosol absorption. In addition, the oxygen A and B bands can be used to constrain variations of ALH. By making full use of the EPIC measurement information, the accuracy of aerosol retrievals can be significantly improved.

CRediT authorship contribution statement

Lu Gui: Writing – review & editing, Writing – original draft, Validation, Methodology, Conceptualization. **Minghui Tao:** Writing – review & editing, Writing – original draft, Software, Investigation, Formal analysis. **Lina Xu:** Methodology, Investigation, Formal analysis. **Yi Wang:** Software, Project administration, Investigation. **Jun Wang:** Writing – review & editing, Supervision. **Lunche Wang:** Formal analysis, Conceptualization. **Liangfu Chen:** Formal analysis, Conceptualization.

Declaration of competing interest

The authors declare that they have no known competing financial interests or personal relationships that could have appeared to influence the work reported in this paper.

Data availability

Data will be made available on request.

Acknowledgments

This study was supported by National Natural Science Foundation of China (Grant No. 41830109 and 41871262). Jun Wang's participation is made possible via the in-kind support from the University of Iowa. We thank the EPIC team for the data used in our work (https://asdc.larc.nasa.gov/project/DSCOVR). We acknowledge AERONET site PIs (B.N. Holben, H. Chen, L. Wu, R. Ma, J.E. Nichol, P. Wang, X. Xia, and Z. Li) for providing the aerosol data available.

Appendix A. Supplementary data

Supplementary data to this article can be found online at https://doi.org/10.1016/j.atmosres.2024.107268.

References

Ahn, C., Torres, O., et al., 2021. Evaluation of aerosol properties observed by DSCOVR/EPIC instrument from the Earth-Sun Lagrange 1 orbit. J. Geophys. Res. Atmos. 126 (12), e2020JD033651.
Bessho, K., Date, K., et al., 2016. An introduction to Himawari-8/9— Japan&rsquos new-generation geostationary meteorological satellites. J. Meteorol. Soc. Japan. Ser. II 94 (2), 151–183.
Dubovik, O., King, M.D., 2000. A flexible inversion algorithm for retrieval of aerosol optical properties from Sun and sky radiance measurements. J. Geophys. Res. Atmos. 105 (D16), 20673–20696.
Dubovik, O., Holben, B., et al., 2002. Variability of Absorption and Optical Properties of Key Aerosol Types Observed in Worldwide Locations. J. Atmos. Sci. 59 (3), 590–608.
Eck, T.F., Holben, B.N., et al., 1999. Wavelength dependence of the optical depth of biomass burning, urban, and desert dust aerosols. J. Geophys. Res. Atmos. 104 (D24), 31333–31349.
Giles, D.M., Sinyuk, A., et al., 2019. Advancements in the Aerosol Robotic Network (AERONET) Version 3 database – automated near-real-time quality control algorithm with improved cloud screening for Sun photometer aerosol optical depth (AOD) measurements. Atmos. Meas. Tech. 12 (1), 169–209.
Gui, L., Tao, M., et al., 2022. Climatology of aerosol types and their vertical distribution over East Asia based on CALIPSO lidar measurements. Int. J. Climatol. 42 (11), 6042–6054.
Herman, J., Huang, L., et al., 2018. Synoptic ozone, cloud reflectivity, and erythemal irradiance from sunrise to sunset for the whole earth as viewed by the DSCOVR spacecraft from the earth–sun Lagrange 1 orbit. Atmos. Meas. Tech. 11 (1), 177–194.
Hsu, N.C., Jeong, M.J., et al., 2013. Enhanced Deep Blue aerosol retrieval algorithm: The second generation. J. Geophys. Res. Atmos. 118 (16), 9296–9315.
Jethva, H., Torres, O., Ahn, C., 2014. Global assessment of OMI aerosol single-scattering albedo using ground-based AERONET inversion[J]. J. Geophys. Res. Atmos. 119 (14), 9020–9040.
Kaufman, Y.J., Tanre, D., et al., 2002. A satellite view of aerosols in the climate system. Nature 419 (6903), 215–223.
Kim, J., Jeong, U., et al., 2020. New era of air quality monitoring from space: geostationary environment monitoring spectrometer (GEMS). Bull. Am. Meteorol. Soc. 101 (1), E1–E22.
Koffi, B., Schulz, M., Bréon, F.M., et al., 2012. Application of the CALIOP layer product to evaluate the vertical distribution of aerosols estimated by global models: AeroCom phase I results[J]. J. Geophys. Res. Atmos. 117 (D10).
Liu, Z., Liu, D., et al., 2008. Airborne dust distributions over the Tibetan Plateau and surrounding areas derived from the first year of CALIPSO lidar observations. Atmos. Chem. Phys. 8 (16), 5045–5060.
Lu, Z., Wang, J., et al., 2023. First mapping of monthly and diurnal climatology of Saharan dust layer height over the Atlantic Ocean from EPIC/DSCOVR in deep space. Geophys. Res. Lett. 50 (5), e2022GL102552.
Lyapustin, A., Wang, Y., Korkin, S., et al., 2018. MODIS collection 6 MAIAC algorithm [J]. Atmos. Meas. Tech. 11 (10), 5741–5765.
Lyapustin, A., Wang, Y., Go, S., et al., 2021. Atmospheric correction of DSCOVR EPIC: version 2 MAIAC algorithm[J]. Front. Rem. Sens. 2, 748362.
Marshak, A., Herman, J., et al., 2018. Earth observations from DSCOVR EPIC instrument. Bull. Am. Meteorol. Soc. 99 (9), 1829–1850.
Mishchenko, M.I., Cairns, B., et al., 2004. Monitoring of aerosol forcing of climate from space: analysis of measurement requirements. J. Quant. Spectrosc. Radiat. Transf. 88 (1), 149–161.
Mishchenko, M.I., Geogdzhayev, I.V., et al., 2007. Past, present, and future of global aerosol climatologies derived from satellite observations: a perspective. J. Quant. Spectrosc. Radiat. Transf. 106 (1–3), 325–347.
Pope, I.C., Burnett, R.T., et al., 2002. Lung cancer, cardiopulmonary mortality, and long-term exposure to fine particulate air pollution. JAMA 287 (9), 1132–1141.
Tao, M., Wang, J., et al., 2019. Performance of MODIS high-resolution MAIAC aerosol algorithm in China: characterization and limitation. Atmos. Environ. 213, 159–169.
Tao, M., Wang, J., et al., 2020. Characterization of aerosol type over East Asia by 4.4 km MISR product: first insight and general performance. J. Geophys. Res. Atmos. 125 (13), e2019JD031909.
Tao, M., Gui, L., et al., 2021. Tracking prevailing dust aerosol over the air pollution in Central China with integrated satellite and ground observations. Atmos. Environ. 253, 118369.
Tao, M., Chen, L., et al., 2022. Characterization of dust activation and their prevailing transport over East Asia based on multi-satellite observations. Atmos. Res. 265, 105886.
Torres, O., Tanskanen, A., et al., 2007. Aerosols and surface UV products from ozone monitoring Instrument observations: an overview. J. Geophys. Res. 112 (D24), D24S47.
Torres, O., Ahn, C., et al., 2013. Improvements to the OMI near-UV aerosol algorithm using A-train CALIOP and AIRS observations. Atmos. Meas. Tech. 6 (11), 3257–3270.
Torres, O., Bhartia, P.K., Jethva, H., Ahn, C., 2018. Impact of the ozone monitoring instrument row anomaly on the long-term record of aerosol products. Atmos. Meas. Tech. 11, 2701–2715. https://doi.org/10.5194/amt-11-2701-2018.
Wang, T., Chen, Y., et al., 2020. Assessment of dominating aerosol properties and their long-term trend in the Pan-Third Pole region: a study with 10-year multi-sensor measurements. Atmos. Environ. 239, 117738.
Wang, T., Tang, J., et al., 2021. Identifying a transport mechanism of dust aerosols over South Asia to the Tibetan Plateau: a case study. Sci. Total Environ. 758, 143714.
Xu, X., Wang, J., et al., 2017. Passive remote sensing of altitude and optical depth of dust plumes using the oxygen a and B bands: first results from EPIC/DSCOVR at Lagrange-1 point. Geophys. Res. Lett. 44 (14), 7544–7554.
Xu, X., Wang, J., et al., 2019. Detecting layer height of smoke aerosols over vegetated land and water surfaces via oxygen absorption bands: hourly results from EPIC/DSCOVR in deep space. Atmos. Meas. Tech. 12 (6), 3269–3288.
Zhang, Z., Fan, M., et al., 2019. A simplified aerosol retrieval algorithm for Himawari-8 Advanced Himawari Imager over Beijing. Atmos. Environ. 199, 127–135.